Balancing interpixel cross talk and detector noise to optimize areal density in holographic storage systems

María-P. Bernal, Geoffrey W. Burr, Hans Coufal, and Manuel Quintanilla

We investigate the effects of interpixel cross talk and detector noise on the areal storage density of holographic data storage. A numerical simulation is used to obtain the bit-error rate (BER) as a function of hologram aperture, pixel fill factors, and additive Gaussian intensity noise. We consider the effect of interpixel cross talk at an output pixel from all possible configurations of its 12 closest-neighbor pixels. Experimental verification of this simulation procedure is shown for several fill-factor combinations. The simulation results show that areal density is maximized when the aperture coincides with the zero order of the spatial light modulator (SLM) (Nyquist sampling condition) and the CCD fill factor is large. Additional numerical analysis including finite SLM contrast and fixed-pattern noise show that, if the fixed-pattern noise reaches 6% of the mean signal level, the SLM contrast has to be larger than 6:1 to maintain high areal density. We also investigate the improvement of areal density when error-prone pixel combinations are forbidden by using coding schemes. A trade-off between an increase in areal density and the redundancy of a coding scheme that avoids isolated-ON pixels occurs at a code rate of approximately 83%. © 1998 Optical Society of America

OCIS codes: 210.2860, 040.1520, 050.1220, 070.2580, 070.2590, 050.1960.

1. Introduction

Digital holographic data storage has become the focus of study of many researchers in the past few years[1–8] because of its potential use in storage with fast parallel access and high storage density. The technique consists of storing a large number of digital pages in a thick photosensitive medium as superimposed gratings produced by the interference between coherent object and reference laser beams.

One of the most widely used configurations in holographic data storage is the Fourier transform configuration (a $4f$ system), as shown in Fig. 1. Information to be stored is encoded with a programmable-pixel device, a spatial light modulator (SLM), located in the front focal plane of lens L_1. A collimated and expanded laser beam (the object beam) is transmitted through the SLM and focused with lens L_1 in the photosensitive medium, which for our purposes can be simplified to a square aperture of area D^2. The storage material is placed at or near this Fourier transform plane to maximize areal density. If the SLM pixels could be made extremely small ($\sim$5 μm), an image-plane geometry could become attractive.[9]

A hologram is written when a second coherent laser beam (the reference beam) intersects with the object beam and their interference fringes are recorded as a diffraction grating in the medium. The information-bearing object beam can then be reconstructed by illumination of the stored diffraction grating with the reference beam. By use of a second lens L_2 to perform a second Fourier transformation, the digital information can be retrieved by a CCD camera in parallel. The SLM and the CCD camera are typically pixelated: Each pixel on the SLM has a corresponding pixel on the CCD camera.

The high areal densities needed to make digital holographic data storage a feasible technology are achieved by the superimposition of multiple holograms within the same region of storage material (a stack of holograms). However, the diffraction efficiency of each hologram scales as 1 over the square of the number of overlapping exposures. Therefore it is crucial to minimize the exposure area of each hologram with a small aperture. An aperture also allows reuse of the same set of reference angles–wavelengths in neighboring storage locations without

M.-P. Bernal, G. W. Burr, and H. Coufal are with the IBM Almaden Research Center, 650 Harry Road, San Jose, California 91520-6099. M. Quintanilla is with the Departamento de Física Aplicada, Facultad de Ciencias, Universidad de Zaragoza, 50009 Zaragoza, Spain.

Received 24 December 1997; revised manuscript received 29 April 1998.

0003-6935/98/235377-09$15.00/0

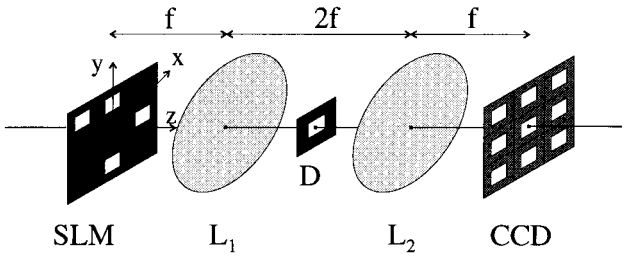

Fig. 1. Schematic of a 4*f* configuration used for holographic data storage.

creating interstack cross talk. However, the small aperture acts to spatially low-pass filter the data-bearing object beam. High-spatial-frequency components of the data pattern displayed on the SLM will not be recorded by the holographic medium. As a result, the light propagated from a SLM pixel is spread to the neighboring pixels of the intended target CCD pixel. Depending on the pattern of the nearby pixels displayed on the SLM, the retrieved data might no longer be able to be decoded correctly.[10–11] This source of deterministic errors is called interpixel cross talk.

For a modest amount of interpixel cross talk, although there could be no decoding errors, the separation between the brightest OFF pixel and the darkest ON pixel is reduced [the signal-to-noise ratio (SNR) is decreased]. Even a small amount of additional random noise (from the detector electronics, for instance) will begin to cause decoding errors. In general, a holographic system that can tolerate more random noise can afford to reduce its signal levels and thus superimpose more holograms. So part of the SNR budget is used to tolerate interpixel cross talk and increase density by minimization of the stack area, and part of the SNR budget is used to tolerate random noise and increase density by an increase in the number of holograms per stack.

In this study we use a numerical algorithm to obtain a set of design parameters that produces a digital holographic data-storage system with the optimal areal density for a given target bit-error rate (BER). We account for several of the important noise sources present in a practical holographic system: deterministic sources of signal variation, such as interpixel cross talk, fixed-pattern noise, and limited SLM contrast, and random noise sources, such as detector noise. The effects of detector alignment and optical aberrations are not included in this analysis. Using these simulations, we can model any linear fill factor in the SLM and in the CCD camera, as well as various spatial cutoff frequencies in the Fourier transform plane.

In Section 2 we describe the numerical algorithm to evaluate the BER as a function of the SLM and the CCD fill factors, the aperture in the Fourier plane, and the relative amount of additive noise. Simulations at several fill-factor combinations are compared with experimental BER measurements to validate the approach. Simulated BER maps for the full range of fill-factor choices indicate that each aperture has its own best SLM and CCD fill-factor combination. By relating the amount of random noise to the number of holograms that can be stored, we determine the areal density as a function of the target BER. We show that density is maximized by pushing the system toward the Nyquist sampling condition and that large SLM and CCD fill factors are appropriate for systems dominated by detector noise. The effects of finite SLM contrast and fixed-pattern noise are then included, and the possible benefits of low-pass modulation coding are evaluated.

2. Review of the Method

Our numerical algorithm considers the system model described in Fig. 1. Lenses L_1 and L_2 form a 4*f* system of unity magnification that images the SLM exactly onto the CCD detector array. We assume a SLM with pixels of a linear dimension Γ and a linear fill factor g_{SLM}, a CCD camera also with pixels of an identical linear dimension Γ but a linear fill factor g_{CCD}, and a square aperture of area D^2 located in the common focal plane of lenses L_1 and L_2. We assume that the system has a space-invariant impulse response (point-spread function) that is due solely to the aperture. The possible effects of magnification, focus, and registration errors and of lens aberrations are not included.

For uniform plane-wave illumination and a linear fill factor g_{SLM}, the transmission-field amplitude of a single SLM pixel centered at the optical axis is given by

$$U_0(x, y, z = 0) = \mathrm{rect}\left(\frac{x}{g_{\mathrm{SLM}}\Gamma}\right)\mathrm{rect}\left(\frac{y}{g_{\mathrm{SLM}}\Gamma}\right). \quad (1)$$

By use of the Rayleigh–Sommerfeld diffraction theory,[12] the electric-field amplitude in the Fourier transform plane of lens L_1 is the two-dimensional (2-D) spatial Fourier transform of Eq. (1):

$$Uc(x, y, z = 2f) = \frac{{g_{\mathrm{SLM}}}^2\Gamma^2}{i\lambda f}\,\mathrm{sinc}\left(\frac{g_{\mathrm{SLM}}\Gamma x}{\lambda f}\right)\mathrm{sinc}\left(\frac{g_{\mathrm{SLM}}\Gamma y}{\lambda f}\right), \quad (2)$$

where λ is the laser wavelength and f is the focal length of lenses L_1 and L_2. If these lenses are assumed to be diffraction limited and of infinite extent, the range of frequency components that are stored in the medium is limited by the square aperture of linear dimension D (located in the back focal plane of L_1), which can be expressed mathematically as

$$P(x, y) = \mathrm{rect}\left(\frac{x}{D}\right)\mathrm{rect}\left(\frac{y}{D}\right). \quad (3)$$

The electric-field amplitude at the CCD can be obtained directly by the application of the scalar diffraction theory again:

$$U_d(x, y, z = 4f) = -{g_{\mathrm{SLM}}}^2\Gamma^2 I(x)I(y), \quad (4)$$

where

$$I(v) = \int_{-\alpha}^{+\alpha} \mathrm{sinc}(\Gamma g_{\mathrm{SLM}} s)\exp(-i2\pi v s)\mathrm{d}s,$$

$$\alpha \equiv \frac{D}{2\lambda f}. \tag{5}$$

So $U_d(x, y, z = 4f)$ is the pixel-spread function: the field distribution along the x–y direction in the CCD plane resulting from a single SLM pixel of linear fill factor g_{SLM} centered at $x = y = 0$ and an aperture of linear width D. By use of the convolution theorem, this can be described as the convolution of the point-spread function [the Fourier transform of Eq. (3)] with the original pixel shape [Eq. (1)]. There is a particular choice of aperture D that will become important in the simulation: $D = \lambda f/\Gamma \equiv D_N$. If the aperture is thought of as a low-pass filter of bandwidth $D_N/2$ and the pixel spacing at the CCD camera as a sampling at the frequency $\lambda f/\Gamma$, then the aperture D_N corresponds to the Nyquist sampling condition. With temporal signals this condition is usually met if one chooses to sample at twice the low-pass filter bandwidth. In this context the sampling rate is fixed by the CCD pixel spacing, and it is the low-pass filter of aperture D_N that is chosen. In describing our simulation results, we describe aperture sizes in terms of the ratio D/D_N. This allows the results to be independent of the particular choice of λ, f, and Γ up to the point at which an absolute areal density is evaluated.

In our simulation this pixel-spread function is evaluated by a 2-D fast Fourier transform, a 2-D low-pass operation, and a second 2-D fast Fourier transform for one pixel. The input SLM pixel is represented as a grid of 51×51 subpixels centered at $x = y = 0$. A large number of subpixels ensures the accuracy of the algorithm[11] and increases the number of fill factors that can be simulated. This ON pixel is surrounded by 10 OFF pixels (51×51 subpixels each) to increase the resolution with which the aperture can be specified. The limit on the total number of input subpixels is the memory requirement of the fast Fourier transform. After the space-invariant pixel-spread function has been evaluated for a particular SLM fill factor g_{SLM} and aperture D, the next step is to use linear superposition to synthesize the response at the CCD to an arbitrary input pattern of neighboring pixels on the SLM.

In previous studies of interpixel cross talk[10,11] only the influence of the four closest neighboring SLM pixels was considered. In this paper we investigate the interpixel cross talk when the 12 nearest neighboring SLM pixels are taken into account. A schematic of our procedure is shown in Fig. 2. As the field at the CCD plane for a single SLM pixel is known [Eq. (4)], evaluation of the field at the target CCD [pixel (0, 0)] is simple. For each of the 13 pixels under consideration the electric-field distribution for the pixel-spread function is translated by the appropriate pixel increment,

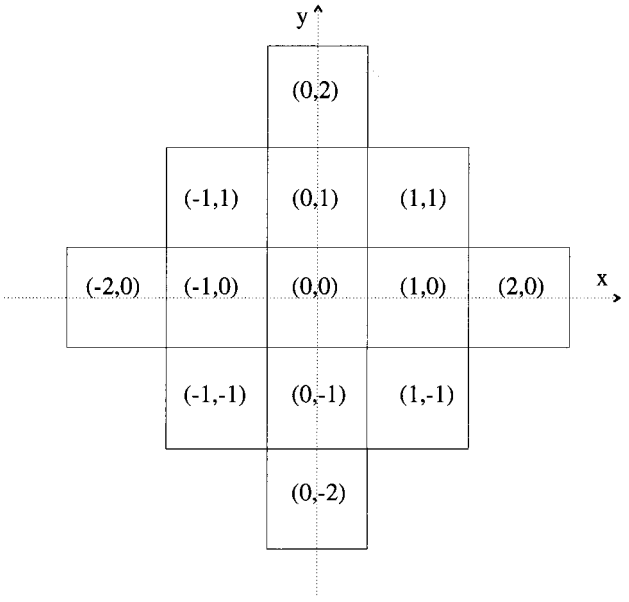

Fig. 2. Thirteen-pixel pattern used to study interpixel cross talk. The coherent contribution of these 12 nearest neighbors is evaluated over the central pixel.

multiplied by the corresponding SLM brightness value, and summed at the subpixel level. This results in the total amplitude distribution over the 51×51 subpixels of the central CCD pixel. Integrating the output intensity over the square subpixel area defined by the CCD linear fill factor g_{CCD} gives the signal seen by the CCD pixel at that particular fill factor.

It is important to note that we are normalizing the integrated intensity over a single pixel-spread function to 1, independently of the aperture or the SLM fill factor. That is, reduction in the CCD pixel signal value can come from a low CCD fill factor but not from having a small aperture or a low SLM fill factor. In practice, this implies that a small aperture or a low SLM fill factor is counteracted by longer hologram exposures, so the same diffraction efficiency is reached in the end. When the $M/\#$ of the system (which is the constant of proportionality between the diffraction efficiency and the number of holograms squared) is independent of the aperture (transmission geometry but not 90° geometry),[13] the result is a loss of recording rate but not of dynamic range.

Mathematically the superposition procedure can be expressed as follows: The brightness of the (i, j)th SLM pixel is written as c_{ij}. Initially, we assume a SLM contrast of infinity, so c_{ij} takes only the value 0 or 1. The amplitude-field distribution at $(x, y, z = 4f)$ in the CCD plane is given by

$$\begin{aligned} U_T(x, y) = {} & c_{02}U_d(x, y + 2\Gamma) + c_{-20}U_d(x - 2\Gamma, y) \\ & + \sum_{i=-1}^{1}\sum_{j=-1}^{1} c_{ij}U_d(x - i\Gamma, y - j\Gamma) \\ & + c_{20}U_d(x + 2\Gamma, y) + c_{0-2}U_d(x, y - 2\Gamma). \end{aligned} \tag{6}$$

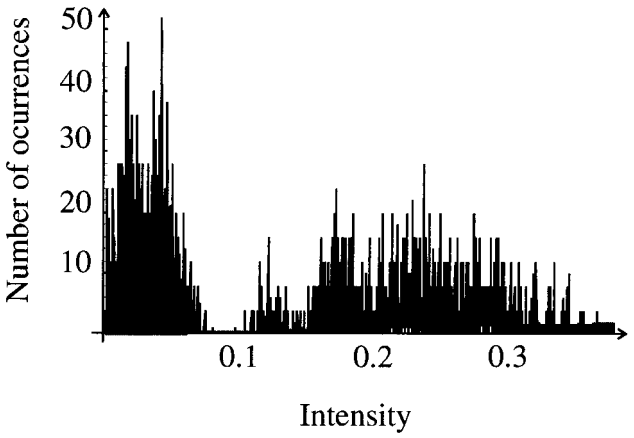

Fig. 3. Example of a discrete histogram for SLM and CCD fill factors of 100% and the Nyquist aperture.

The signal received by the target CCD pixel with a linear fill factor g_{CCD} is obtained as

$$I_T = \sum_{x_m=-g_{\mathrm{CCD}}\Gamma/2}^{+g_{\mathrm{CCD}}\Gamma/2} \sum_{y_m=-g_{\mathrm{CCD}}\Gamma/2}^{+g_{\mathrm{CCD}}\Gamma/2} |U_T(x_m, y_m, z = 4f)|^2. \quad (7)$$

The quantum efficiency for the detection of photons in the CCD and other scaling factors are omitted. The value of I_T in Eq. (7) is the received signal for a particular 13-pixel pattern combination at the SLM described by the c_{ij} values of Eq. (6). The next step is to evaluate the intensity of all the 2^{13} equally likely combinations and build a discrete histogram.

The 2^{13} possible combinations are separated into two classes according to the state of the central (desired) SLM pixel, and occurrences are accumulated in a finite number of brightness bins. Figure 3 shows an example of a discrete histogram for the case of both SLM and CCD fill factors equaling 100% and at the Nyquist aperture. The bin size was 1/1000 of the normalized intensity. The histogram shows deterministic variations coming from interpixel cross talk. If the aperture were made large, the histogram would coalesce to two delta functions, located at 0 and 1. However, the histograms shown in Fig. 3 are not representations of a probability density function: More samples will not reveal previously hidden structure at the tails of the distribution. If the two intensity distributions do not overlap, they will never overlap. However, ON and OFF intensity distributions that are far away from each other seem more desirable than those that are close but do not overlap.

The reason for this is that all systems are subject to random fluctuations, either quantum (shot noise) or thermal (Johnson noise). In practical holographic systems the noise associated with detector electronics tends to overshadow the shot noise. This noise source can be modeled with Gaussian statistics.[14] Thus, to represent the statistical fluctuation from random noise, we convolve each intensity bin in the discrete histogram with a Gaussian distribution of standard deviation σ_d. The standard deviation σ_d is expressed as a percentage of the incoming signal level (that is, normalized to 1.0 on our histogram's x axis). Now we have real probability density functions for both distributions and can derive the BER.

If there are N_0 bins corresponding to the histogram of a target OFF pixel, we call $\{w_{i,0}\}_{i=1,N_0}$ the number of counts in the bin at the intensity value $\{\mu_{i,0}\}_{i=1,N_0}$. The variables N_1, $\{w_{i,1}\}_{i=1,N_1}$, and $\{\mu_{i,1}\}_{i=1,N_1}$ are defined analogously for the ON distribution. So we have a set of shifted and scaled equal-variance Gaussians, with μ_{ij} describing the shifting and w_{ij} the scaling.

If the total number of counts in each distribution is d_0 and d_1, i.e., $d_0 = \Sigma_{i=1}^{N_0} w_{i,0}$ and $d_1 = \Sigma_{i=1}^{N_1} w_{i,1}$, the BER with a threshold of intensity Θ is given by

$$\mathrm{BER} = \frac{1}{4}\left[\frac{1}{d_0}\sum_{i=1}^{N_0} w_{i,0}\,\mathrm{erfc}\left(\frac{\Theta - \mu_{i,0}}{\sqrt{2}\sigma_d}\right) + \frac{1}{d_1}\sum_{i=1}^{N_1} w_{i,1}\,\mathrm{erfc}\left(\frac{\mu_{i,1} - \Theta}{\sqrt{2}\sigma_d}\right)\right], \quad (8)$$

where erfc is the complementary error function.[15] For given ON and OFF distributions the BER depends on the selected threshold intensity Θ. To obtain the minimum BER for each situation, we evaluated Eq. (8) repeatedly until the best value of Θ was found.

In summary, this numerical procedure evaluates the BER, given four dimensionless input parameters:

1. A linear SLM fill factor g_{SLM}, expressed as a fraction of Γ.
2. An aperture size D, expressed as a fraction of D_N.
3. A linear CCD fill factor g_{CCD}, expressed as a fraction of Γ.
4. Additive detector noise σ_d, expressed as a fraction of the signal strength in an ideal system (no cross talk and a 100% fill factor).

3. Experimental Validation

To verify the results of our simulations, we measured the BER as a function of aperture size experimentally for some specific SLM–CCD fill factors in a photorefractive information-storage material (PRISM) tester.[6] The SLM was a chrome-on-glass mask with 100% and 50% linear fill factors, and the CCD camera had a 100% fill factor.

The results are shown in Fig. 4, with the BER shown as a function of the aperture (in units of the Nyquist aperture). Note that, with a focal length of 89 mm, a pixel spacing of 18 μm, and a 514.5-nm wavelength, the Nyquist aperture corresponds to 2.54 mm in real units. Figure 4(a) corresponds to the case of both SLM and CCD fill factors equaling 100%, and in Fig. 4(b) the linear SLM fill factor is equal to 50%. In both situations a value of σ_d could be found at which simulation and experiment showed excellent agreement. When the SLM and the CCD fill factors were both 100%, the BER increased monotonically as the aperture size decreased. However, if the SLM fill factor was smaller than 100%, the BER

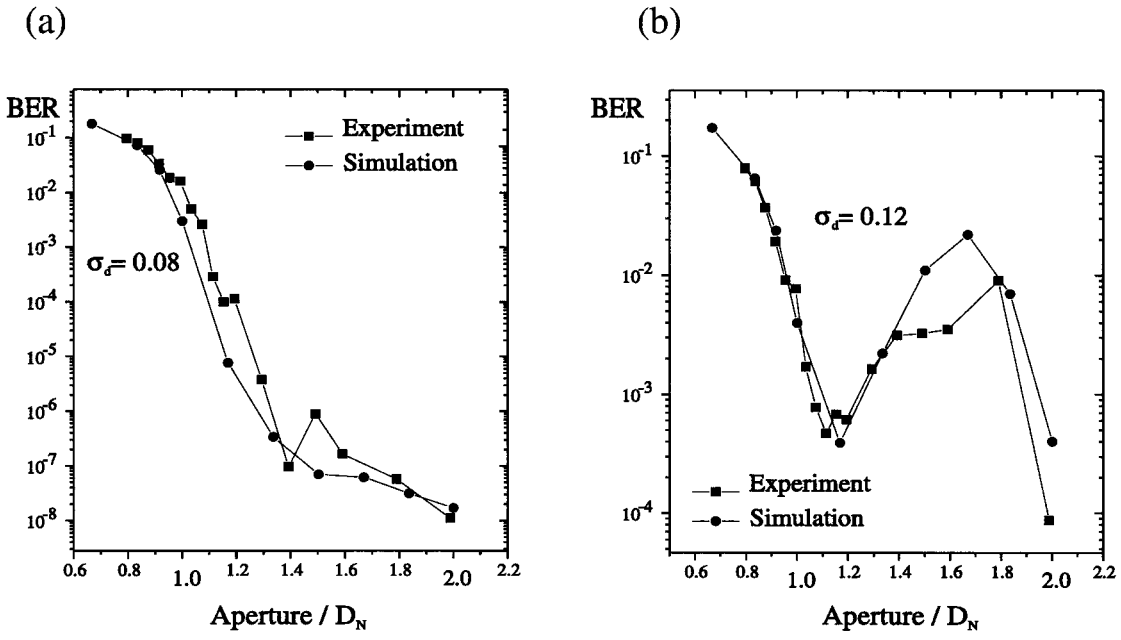

Fig. 4. Experimental validation of the proposed algorithm. Experiments on the BER versus the aperture were performed in the PRISM tester for two situations: (a) SLM and CCD fill factors of 100%. (b) SLM linear fill factor of 50% and CCD fill factor of 100%.

initially increased, then passed through a local minimum in the BER at 1.08 times the Nyquist aperture, and finally increased rapidly for smaller apertures. This is because the Fourier transform consists of a set of multiple orders at regular spacing, each one containing the complete information of the data page and weighted by the sinc pattern of one pixel. At the Nyquist aperture all the orders except the zero order are blocked, whereas at apertures larger than the Nyquist aperture there exists a competition between the zero order of the SLM and incomplete copies of the various ± 1 orders [Fig. 4(b)].

4. Bit-Error Rate Maps and Areal Density

Figure 4 provides evidence that our numerical procedure provides an accurate representation of real holographic systems and shows that there is a difference in the behavior of the BER as the SLM–CCD fill factors vary. To investigate this difference further, we computed the BER for a small set of apertures but varied the SLM and the CCD fill factors over a large number of possible values. A constant amount of detector noise relative to the signal level was assumed.

The results are shown in Fig. 5. Contour plots of the BER as a function of the SLM and the CCD linear fill factors are shown for two different apertures: the Nyquist aperture and twice the Nyquist aperture. For small BER values the contour lines are not smooth because of the inaccuracy of the numerical algorithm. Detector noise of 5% was assumed (that is, the standard deviation of the additive Gaussian noise was 5% of the no-cross-talk ON signal level). Two interesting effects can be seen from the results. As the aperture increases, the location of the minimum BER moves from small to large SLM fill factors, whereas large CCD fill factors are always advantageous. At the Nyquist aperture, the minimum BER was approximately 10^{-6}, whereas at twice the Nyquist aperture it was of the order of 10^{-20}. Apparently, having a large aperture tends to be beneficial because the system can tolerate more additive noise before reaching the target BER. For a practical system this target BER is dictated by the error-correction coding and tends to be approximately 10^{-3}–10^{-4}. Depending on one's frame of reference, more additive noise can mean either increased noise and constant signal strength (like our model) or decreased signal strength and a constant noise floor (like the physical holographic system). If the aperture is large more detector noise (or equivalently, lower signal levels) could be tolerated, and therefore more holograms could be stored. Therefore on the basis of Fig. 5 it is necessary to quantify these concepts to understand the trade-off between the number of holograms and the aperture size in terms of areal density. To obtain a value of the areal density (the number of stored bits per area) for a given BER target, we returned to the numerical method described in Section 2. We reiterate our assumptions:

(a) The location of the aperture is exactly at the Fourier plane.

(b) Only detector and interpixel cross-talk noise are included. Noise sources such as interpage or interstack noise are not considered in this numerical study.

(c) No optical aberrations are taken into account in the optical system (the point-spread function is assumed to be space invariant).

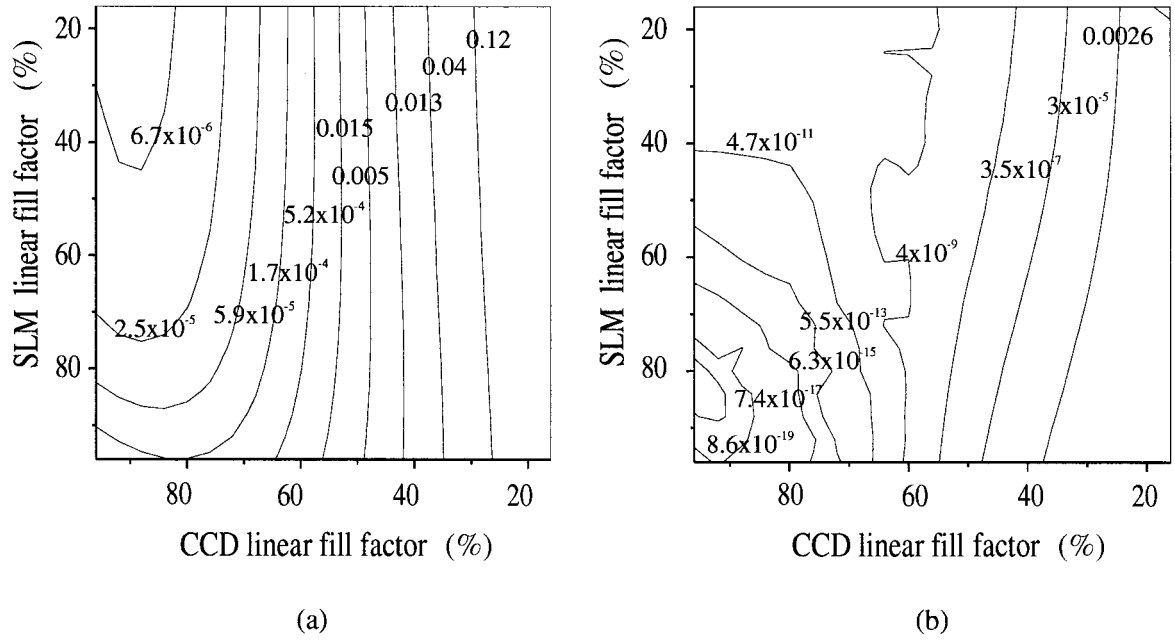

Fig. 5. BER as a function of the CCD and the SLM linear fill factors for (a) the Nyquist aperture and (b) twice the Nyquist aperture. The detector-noise level is 5% of the incoming signal level (before losses derived from diffraction and CCD dead space).

To solve for the areal density, it is assumed that we stop recording holograms when

$$n_d = \sigma_d n_s, \tag{9}$$

where n_d is the number of detector-noise electrons per pixel, n_s is the number of signal electrons detected by a CCD pixel, and σ_d is the relative standard deviation of the detector noise at which the BER hits the target level (of the order of 1%–10%). The procedure is to select a set of fill factors and an aperture and increase σ_d until our numerical simulation indicates that the target BER has been reached. Given a detector-noise specification (say, 100 noise electrons), we can solve for the minimum number of signal electrons we must have. To relate this to readout power and integration time, we write the number of signal electrons per ON pixel as

$$n_s = \left(\frac{P_{\text{ref}}}{h\nu}\right) \eta_{\text{hologram}} \eta_{\text{opt}} \eta_e t_{\text{int}} \frac{1}{N_{\text{ON}}}, \tag{10}$$

where N_{ON} is the number of ON pixels in the SLM, which, assuming half of the total number of pixels N_p is ON, can be replaced by $N_p/2$. The term $P_{\text{ref}}/h\nu$ is the number of photons per second in the reference beam, η_{hologram} is the diffraction efficiency of the holograms, η_{opt} is the efficiency of the optical system, which includes all the optical losses between the media and the camera (but not the dead spaces from the CCD pixel fill factors), η_e is the camera quantum efficiency, and t_{int} is the integration time of the camera.

In addition, the diffraction efficiency of the holograms can be expressed in terms of the $M/\#$ of the holographic system and the number of stored holograms M,[13] as

$$\eta_{\text{hologram}} = \left(\frac{M/\#}{M}\right)^2. \tag{11}$$

Equation (10) tells us how many signal electrons we must have to overcome both the detector noise and the interpixel cross talk. Equations (10) and (11) indicate how P_{ref}, the $M/\#$, and the number of holograms M influence the number of signal electrons. Combining Eqs. (9)–(12), we derive the number of holograms M in terms of σ_d, η_e, $M/\#$, P_{ref}, and t_{int}:

$$M \sim M/\# \left(\frac{\sigma_d}{n_d} \frac{P_{\text{ref}}}{h\nu} t_{\text{int}} \frac{2}{N_p} \eta_e \eta_{\text{opt}}\right)^{1/2}. \tag{12}$$

As expected, a higher $M/\#$, more readout power, or more integration time means more holograms can be stored. The effect of a smaller aperture arises through a smaller σ_d value from the simulation. In effect, a larger portion of the SNR budget goes to interpixel cross talk, leaving less for detector noise and thus reducing M.

However, a smaller aperture may be better in terms of areal density:

$$\mathcal{D} = \frac{\left(\frac{\text{number of pixels}}{\text{hologram}}\right)(\text{number of holograms})}{\text{aperture area}}. \tag{13}$$

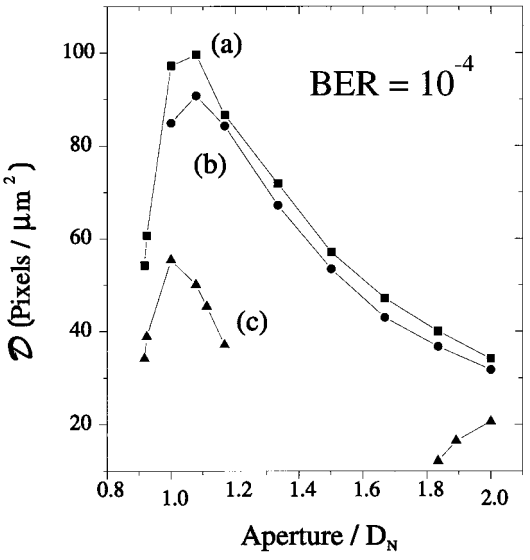

Fig. 6. Areal density as a function of the aperture for (a) the best combination of fill factors (obtained with BER maps such as those shown in Fig. 5), (b) a SLM linear fill factor of 90% and a CCD linear fill factor of 87%, and (c) a SLM linear fill factor of 60% and a CCD linear fill factor of 40% (corresponding to the DEMON system[8]).

Substituting Eq. (12) into Eq. (13) yields the areal density in the form

$$\mathcal{D} = \frac{M/\#\left(N_p \frac{P_{\text{ref}}}{h\nu}\frac{\sigma_d}{n_d}\eta_{\text{opt}}\eta_e t_{\text{int}} 2\right)^{1/2}}{D^2}. \qquad (14)$$

To verify that Eq. (14) has validity, we can try to predict the areal density achieved in the DEMON (demonstration platform) system.[8] In this system 1200 holograms were superimposed, with 46,000 user bits/hologram. Although a large aperture was used in the demonstration, recent results show that an identical performance could be expected with an aperture as small as 5 mm. This is an achieved areal density of 2.2 bits/μm^2. By putting the parameters for this demonstration into Eq. (14), i.e., $M/\# \sim 0.2$, $N_p = 320 \times 240$, $P_{\text{ref}} \sim 200$ mW, $\sigma_d \sim 0.033$, $n_d \sim 100e^-$, $\eta_{\text{opt}} \sim 0.4$, $\eta_e \sim 0.3$, $t_{\text{int}} \sim 0.016$ s, and $D \sim 5$ mm, we obtain 1.9 bits/μm^2. So there is some support for using Eq. (14) to predict absolute areal densities.

In Fig. 6 the areal density achievable at a BER of 10^{-4} is shown as a function of the aperture (in units of the Nyquist aperture) for three different SLM–CCD design parameters. For curve (a) each data point has its own unique SLM–CCD fill-factor pair that gives the minimum BER for that aperture, as obtained from BER maps like those in Fig. 5. The other two curves show the density with a fixed pair of fill factors: large SLM and CCD fill factors (90% and 87%, respectively) for curve (b) and small SLM and CCD fill factors for curve (c). None of the curves shown in Fig. 6 includes any effects from aberrations, interpage cross talk, or interstack cross talk, and they all use the following holographic-system parameters: $M/\# = 0.94$, $P_{\text{ref}} = 200$ mW, $N_p = 10^6$, $n_d = 115e^-$, $\lambda = 514.5$ nm, $t_{\text{int}} = 1$ ms, BER $= 10^{-4}$, and $D = 2$ mm.

The maximum areal density is achieved when the aperture is slightly larger (1.08×) than the Nyquist aperture, the SLM has a 40% linear fill factor, and the detector array has an 88% linear fill factor, and it corresponds to a number of holograms equal to 400 (by use of the parameters described above). However, if large SLM and CCD fill factors are used [curve (b)], Fig. 6 shows that the best areal density (also located at 1.08 times the Nyquist aperture) is just 10% lower than the maximum of curve (a). When the CCD fill factor is small, as shown by curve (c), the maximum areal density is almost 50% lower than for the case depicted by curve (a). In addition, for the case represented by curve (c) there are aperture sizes for which it is not possible to attain the target BER of 10^{-4}. As expected, for apertures smaller than the Nyquist aperture not all the SLM information is transmitted through the aperture, and a low BER cannot be achieved even for a few holograms.

In summary, our simulations show that areal density is maximized by use of the Nyquist aperture and large CCD fill factors, but it is reasonably independent of the SLM fill factors. Given this latter ambiguity, it is desirable to have large SLM fill factors to decrease the recording rate and improve the optical efficiency in the object beam.

5. Spatial Light Modulator Contrast and Fixed-Pattern Noise

All the simulations up to this point assumed that the SLM has infinite contrast, that is, the intensity of the OFF pixels is zero at the SLM. In a real holographic device the OFF pixels always transmit some light. For example, the Epson liquid-crystal SLM in the DEMON platform[8] has an ON–OFF contrast ratio of 25:1. Therefore it is important to include the effects of finite SLM contrasts on the areal density. In addition, we introduce a second deterministic noise source, fixed-pattern noise, which comes from spatial variations in the ON level across the SLM.[16] Thus identical pixel patterns can have different intensities in the CCD plane, depending on their locations within the SLM page. This is a problem because the last step in most detection schemes is the thresholding of a small block of pixels by a common threshold.[8,17] This threshold can be calculated explicitly or it can be an implicit by-product of the modulation decoder. Spatial variations within the pixel block will tend to broaden the ON and the OFF distributions seen by the threshold and thus increase the BER.

To include fixed-pattern noise in our system model, we convolve the bins of the discrete histograms corresponding to a target ON pixel with a Gaussian with a larger standard deviation than before. Because fixed-pattern noise is a truly deterministic pattern noise, this convolution can be done only if global thresholding is assumed. For local thresholding the

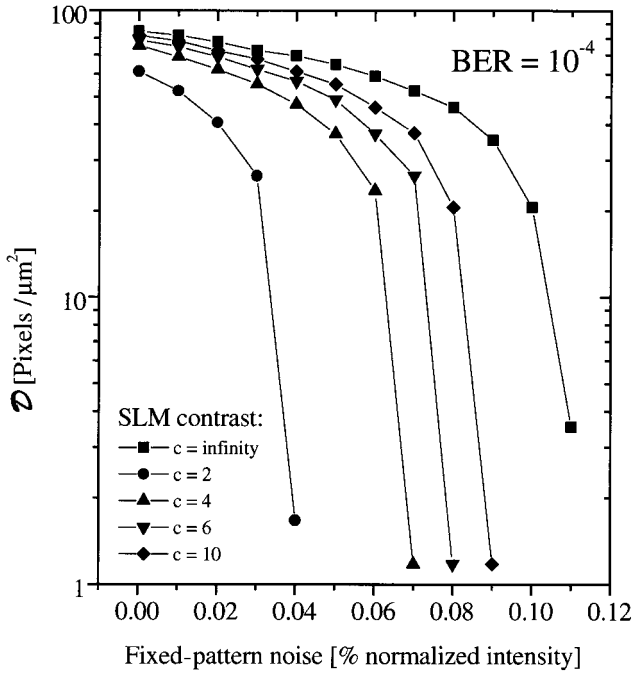

Fig. 7. Areal density as a function of the fixed-pattern noise for different SLM contrast levels at the Nyquist aperture and with large fill factors (SLM, 90%; CCD, 87%).

mean of the intensity values, as well as the standard deviations of the different blocks, would change.

Therefore for global thresholding we have

$$\sigma_{\text{ON}} = \sigma_d + \sigma_p, \tag{15}$$

where σ_d is the standard deviation of the detector noise and σ_p is the standard deviation of the deterministic pattern noise. Both are expressed as functions of the no-cross-talk, no-noise signal level.

Similarly, the bins of the discrete histograms corresponding to a target OFF pixel are convolved with a Gaussian of standard deviation

$$\sigma_{\text{OFF}} = \sigma_d + \sigma_p/c, \tag{16}$$

where c is the SLM contrast (the ratio between the intensity of the ON and the OFF pixels) at the SLM. The BER is then computed by use of the procedure described above. BER maps similar to those shown in Fig. 5 show that, when fixed-pattern noise and SLM contrast are introduced, the BER values rise but the location of the minimum remains invariant (the best-case fill factors are unchanged).

The effects of fixed-pattern noise and the contrast ratio are shown in Fig. 7. The areal density is shown as a function of the fixed-pattern noise. The absolute parameters used are the same as for Fig. 6. The numerical simulations were done at the Nyquist aperture with a 90% SLM linear fill factor and an 87% CCD linear fill factor. Contrasts of infinity, 10, 6, 4, and 2 are compared. When there is no fixed-pattern noise in the holographic system, the areal density does not change substantially for different SLM contrasts. However, as the fixed-pattern noise increases, the effect of the SLM contrast on the areal density at a given BER is dramatic. Figure 7 demonstrates that, if the holographic data-storage system can tolerate 6% fixed-pattern noise, a contrast of at least 6:1 would be needed to maintain high areal density. Alternatively, the recently developed predistortion technique could allow one to reduce the deterministic contributions of both intersymbol interference and fixed-pattern noise.[16] This was demonstrated experimentally for small fill factors,[16] but its success for large fill factors will depend on the tradeoff between equalizing the ON pixel response and minimizing additional diffraction into the OFF pixels.

6. Low-Pass Coding

Interpixel cross-talk studies from previous reports[10,11] indicate that ON pixels surrounded by four adjacent OFF pixels and OFF pixels surrounded by four adjacent ON pixels are the first candidates for producing errors in reconstructed holograms. In those previous studies the intensity value at the target CCD pixel was evaluated, but no value for the BER was derived. As described in Sections 3 and 4, we developed algorithms that can evaluate the BER. We used these algorithms to compute the areal density for the case of the Nyquist aperture and for large SLM and CCD fill factors (90% and 87%, respectively) when those isolated-ON and isolated-OFF SLM combinations are forbidden (by use of suitable coding schemes). The rest of the pixels in the 13-pattern combinations were allowed to have all possible binary combinations. Such a coding scheme[18] is advantageous only if the gain in areal density is larger than the inverse of the code rate (there is no point, for example, in a 50% code rate for a 5% density improvement). The results—the areal density as a function of the BER—are shown in Fig. 8. The curves represent (a) no forbidden patterns, (b) both isolated-ON and isolated-OFF forbidden pixels, and (c) only isolated-ON forbidden pixels. The absolute parameters used for the evaluation of the areal density are the same as in Sections 3 and 4. According to our simulations, avoiding the isolated-OFF pixels seemed to have a negligible effect on the areal density improvement. The similarity between curves (b) and (c) implies that the isolated-ON combination has the greater effect on the BER. Furthermore, according to our simulations, in the range of relevant BER values (10^{-7}–10^{-4}) the overall areal density increases if the code rate for avoiding isolated-ON pixels is larger than 83%.

7. Conclusions

We have developed a numerical method that evaluates the BER of a holographic data-storage system in a 4f configuration for a given SLM fill factor, a given CCD fill factor, and an aperture in the Fourier plane. Interpixel cross talk, detector noise, fixed-pattern noise, and a finite SLM contrast have been considered. Experiments measuring the BER as a function of aperture size for several SLM–CCD fill-factor

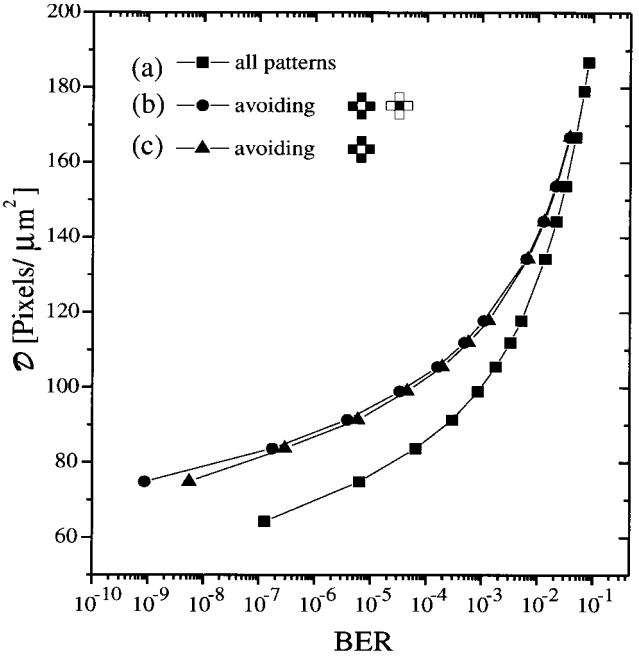

Fig. 8. Areal density as a function of the BER with the Nyquist aperture and large fill factors (SLM, 90%; CCD, 87%) when (a) all possible 13-pixel pattern combinations are considered, (b) all the combinations with an isolated-ON pixel (the four closest neighbors to the center are OFF) are forbidden, and (c) both isolated-ON and isolated-OFF pixels (central pixels OFF; four nearest neighbors ON) are forbidden.

combinations showed excellent agreement with our simulations.

Areal densities for a target BER have been computed for different design parameters by quantification of the trade-off between the number of holograms and the aperture size. Results from the simulations showed that high areal densities could be achieved if the Nyquist aperture and large CCD fill factors were used. (The Nyquist aperture is the same size as the zero order of the SLM's Fourier transform.)

Further studies with a varying SLM contrast have also been carried out. According to the simulations, if the holographic system contains 6% fixed-pattern noise, SLM contrasts of at least 6:1 will be needed to maintain high areal density. In addition, we have analyzed the effects on the areal density when isolated-ON and isolated-OFF SLM combinations were forbidden with appropriate coding schemes. According to our simulations, only the isolated-ON pixel affected the final BER substantially. To realize an increase in the areal density by elimination of these combinations, it would be necessary to have code rates greater than 83%.

This research was partially supported by the U.S. Defense Advanced Research Projects Agency under agreement MDA972-95-0004. We thank in particular the Holographic Optical Storage Tester (HOST) team at the IBM Almaden Research Center for very helpful discussions.

References

1. L. Hesselink and M. Bashaw, "Optical memories implemented with photorefractive media," Opt. Quantum Electron. **25,** 611–651 (1993).
2. F. Mok, "Angle-multiplexed storage of 5000 holograms in lithium niobate," Opt. Lett. **18,** 915–917 (1993).
3. J. Heanue, M. Bashaw, and L. Hesselink, "Volume holographic storage and retrieval of digital data," Science **265,** 749–752 (1994).
4. G. Sincerbox, "Holographic storage revisited," in *Current Trends in Optics*, J. C. Dainty, ed. (Academic, New York, 1994), pp. 195–207.
5. G. W. Burr, F. H. Mok, and D. Psaltis, "Angle and space multiplexed holographic storage using 90 degree geometry," Opt. Commun. **117,** 49–55 (1995).
6. M.-P. Bernal, H. Coufal, R. K. Grygier, J. A. Hoffnagle, C. M. Jefferson, R. M. Macfarlane, R. M. Shelby, G. T. Sincerbox, P. Wimmer, and G. Wittmann, "A precision tester for studies of holographic optical storage materials and recording physics," Appl. Opt. **35,** 2360–2373 (1996).
7. G. W. Burr, F. H. Mok, and D. Psaltis, "Storage of 10,000 holograms in $LiNbO_3$:Fe," in *Conference on Lasers and Electro-Optics*, Vol. 7 of 1994 OSA Technical Digest Series (Optical Society of America, Washington, D.C., 1994), paper CMB7, p. 9.
8. G. W. Burr, J. Ashley, H. Coufal, R. K. Grygier, J. A. Hoffnagle, C. M. Jefferson, and B. Marcus, "Modulation coding for pixel-matched holographic data storage," Opt. Lett. **22,** 639–641 (1997).
9. G. Barbastathis, "Intelligent holographic databases," Ph.D. dissertation (California Institute of Technology, Pasadena, Calif., 1998).
10. J. Hong, I. McMichael, and J. Ma, "Influence of phase masks on cross talk in holographic memory," Opt. Lett. **21,** 1694–1696 (1996).
11. M.-P. Bernal, G. W. Burr, H. Coufal, R. K. Grygier, J. A. Hoffnagle, C. M. Jefferson, E. Oesterschulze, R. M. Shelby, G. T. Sincerbox, and M. Quintanilla, "Effects of multilevel phase masks on interpixel cross talk in digital holographic data storage," Appl. Opt. **36,** 3107–3115 (1997).
12. J. W. Goodman, *Introduction to Fourier Optics* (McGraw-Hill, New York, 1968).
13. G. W. Burr, "Volume holographic storage using the 90° geometry," Ph.D. dissertation (California Institute of Technology, Pasadena, Calif., 1996).
14. G. P. Agrawal, *Fiber-Optic Communication Systems* (Wiley, New York, 1992).
15. W. H. Press, B. P. Flannery, S. A. Teukolsky, and W. T. Vetterling, *Numerical Recipes* (Cambridge U. Press, New York, 1989).
16. G. W. Burr, H. Coufal, R. K. Grygier, J. A. Hoffnagle, and C. M. Jefferson, "Noise reduction of page-oriented data storage by inverse filtering during recording," Opt. Lett. **23,** 289–291 (1998).
17. J. F. Heanue, M. C. Bashaw, and L. Hesselink, "Channel codes for digital holographic data storage," J. Opt. Soc. Am. A **12,** 2432–2439 (1995).
18. J. Ashley and B. Marcus, "Two-dimensional low-pass filtering codes," IEEE Trans. Commun. **46,** 724–727 (1998).